communications biology

A Nature Portfolio journal

Article

https://doi.org/10.1038/s42003-025-07807-4

Cellular dsRNA interactome captured by K1 antibody reveals the regulatory map of exogenous RNA sensing

JinA Lim [1,10], Namseok Lee [1,10], Seonmin Ju [2,3,10], Jeesoo Kim[2,3], Subin Mun [1], Moonhyeon Jeon [1], Yong-ki Lee [1], Seok-Hoon Lee [4], Jayoung Ku [1], Sujin Kim[1], Sangsu Bae [4,5,6], Jong-Seo Kim [2,3] ✉ & Yoosik Kim [1,7,8,9] ✉

RNA-binding proteins (RBPs) provide a critical post-transcriptional regulatory layer in determining RNA fate. Currently, UV crosslinking followed by oligo-dT pull-down is the gold standard in identifying the RBP repertoire of poly-adenylated RNAs, but such method is ineffective in capturing RBPs that recognize double-stranded RNAs (dsRNAs). Here, we utilize anti-dsRNA K1 antibody immunoprecipitation followed by quantitative mass spectrometry to comprehensively identify RBPs bound to cellular dsRNAs without external stimulus. Notably, our dsRNA interactome contains proteins involved in sensing N^6-methyladenosine RNAs and stress granule components. We further perform targeted CRISPR-Cas9 knockout functional screening and discover proteins that can regulate the interferon (IFN) response during exogenous RNA sensing. Interestingly, most dsRBPs promote IFN-β secretion in response to dsRNA stimulation and act as antiviral factors during HCoV-OC43 infection. Our dsRNA interactome capture provides an unbiased and comprehensive characterization of putative dsRBPs and will facilitate our understanding of dsRNA sensing in physiological and pathological contexts.

Double-stranded RNA (dsRNA) is a common pathogen-associated molecular pattern (PAMP) generated as a by-product during RNA virus replication[1]. To counteract viral invasion, cells have developed a collection of pattern recognition receptors (PRRs) that can recognize and bind to dsRNAs to elicit an innate immune response[2]. Examples of well-known PRRs in mammalian cells include melanoma differentiation-associated protein 5 (MDA5), retinoic acid-inducible gene I (RIG-I), protein kinase R (PKR), and toll-like receptor 3 (TLR3). Upon activation, these dsRNA sensors initiate several cellular responses, such as type I interferon (IFN) production, RNA degradation, and translational repression, collectively suppressing viral replication.

Recently, several reports suggested that the human genome includes a large portion of repeat elements whose RNAs can also adopt a double-stranded secondary structure[3–7]. Some abundant dsRNA-generating repeat elements include short interspersed nuclear elements (SINEs), long interspersed nuclear elements (LINEs), and endogenous retroviruses (ERVs). In addition, mitochondria also generate a substantial amount of cellular dsRNAs via bidirectional transcription of the mitochondrial circular genome[8]. More importantly, these endogenous dsRNAs can interact and activate PRRs just like their viral counterparts, which can lead to fatal consequences[7,9,10]. For example, mitochondrial dsRNAs are elevated in synovial fluids of osteoarthritis patients, tear and saliva of autoimmune Sjögren's disease patients, and blood of Huntington's disease patients[11–13]. Moreover, dysregulation and misrecognition of SINE dsRNAs are associated with the development of Aicardi-Goutières syndrome and age-related macular degeneration[14,15]. Thus, understanding the regulation of cellular dsRNAs holds a key in elucidating the pathogenesis of inflammatory diseases.

[1]Department of Chemical and Biomolecular Engineering, Korea Advanced Institute of Science and Technology (KAIST), Daejeon, 34141, Republic of Korea. [2]Center for RNA Research, Institute for Basic Science, Seoul, 08826, Republic of Korea. [3]School of Biological Sciences, Seoul National University, Seoul, 08826, Republic of Korea. [4]Department of Biomedical Sciences, Seoul National University College of Medicine, Seoul, 03080, Republic of Korea. [5]Medical Research Center of Genomic Medicine Institute, Seoul National University College of Medicine, Seoul, Republic of Korea. [6]Cancer Research Institute, Seoul National University College of Medicine, Seoul, 03080, Republic of Korea. [7]Graduate School of Engineering Biology, KAIST, Daejeon, 34141, Republic of Korea. [8]KAIST Institute for Bio-Century, KAIST, Daejeon, 34141, Republic of Korea. [9]KAIST Institute for Health Science and Technology (KIHST), KAIST, Daejeon, 34141, Republic of Korea. [10]These authors contributed equally: JinA Lim, Namseok Lee, Seonmin Ju. ✉e-mail: jongseokim@snu.ac.kr; ysyoosik@kaist.ac.kr

Aberrant immune activation to cellular self-dsRNAs occurs as these RNAs adopt an A-form helical structure with a deep and narrow major groove that prevents the access of individual nucleotides to RBPs[16]. Consequently, innate immune dsRNA sensors typically recognize the length and structural features, such as 5′ triphosphate, to distinguish self from non-self RNAs[2,17,18]. More importantly, such sequence-independent interaction mechanism is shared by multiple dsRNA-binding proteins (dsRBPs), which result in most of them binding to a similar pool of dsRNAs, such as SINEs and ERVs[19–21]. Thus, multiple dsRBPs will compete for access to their common target dsRNAs[22] and work together to regulate the downstream immune response to the increased levels of cellular dsRNAs. We have recently shown that Staufen1 (STAU1) binds to ERV and SINE dsRNAs and stabilizes them to enhance the downstream IFN response[21]. Moreover, adenosine deaminase acting on RNA 1 (ADAR1) and DExH-Box Helicase 9 (DHX9) work together to prevent the recognition of self-dsRNAs by innate immune sensors in breast cancer cells[23].

Despite the pathological relevance and therapeutic potential of cellular dsRNAs, the repertoire of dsRBPs remains largely elusive. The current gold standard of systemic identification of RBPs relies on ultraviolet (UV) crosslinking and pull-down with oligo-dT beads[24,25]. However, this method cannot be extended to the dsRNA interactome due to low UV crosslinking efficiency between the dsRNA and its binding protein[26]. In addition, dsRNAs are generated from repeat elements that lack poly(A) tails, making the oligo-dT pull-down inadequate for capturing proteins that bind to these RNAs. Studies have shown that many of these dsRNA-generating repeat elements are embedded within mRNAs, such as introns and 3′ UTRs[3,5–7]. However, the conventional oligo-dT pull-down cannot specifically enrich dsRBPs, and additional processes are required to remove RBPs that are bound to single-stranded regions of the mRNA. A recent study utilized biotin-conjugated polyinosinic-cytidylic acid (poly(I:C)) to discover dsRBPs, but it is unclear whether these proteins can bind to cellular dsRNAs and regulate dsRNA sensors in uninfected states[27]. Considering that dsRNAs are abundantly expressed in infected cells, utilizing viral RNA as bait to retrieve viral RNA interactome may provide insights into potential dsRBPs[28,29]. Yet, this approach is still limited because viruses develop various mechanisms to shield their dsRNAs from host proteins in order to evade innate immune activation[30]. Moreover, such method retrieves the virus-specific list of interactors, and it is unclear whether the interactome binds to single-stranded RNAs (ssRNAs) or dsRNAs.

In this study, we report an unbiased analysis of the endogenous dsRNA interactome in proliferating human embryonic kidney 293 T (HEK293T) cells with the goal of analyzing its significance in the modulation of IFN response during exogenous RNA sensing. To this end, we employed an original approach that involved co-immunoprecipitation (co-IP) with an anti-dsRNA K1 antibody followed by quantitative mass spectrometry. To reduce false positives, we performed quantitative mass spectrometry analysis with two additional conditions: 1) treatment with RNase T1 to degrade ssRNAs, and 2) in vitro pull-down with synthetic dsRNA, poly(I:C). We then further assessed the regulatory potential of these putative dsRBPs by implementing targeted CRISPR-Cas9 knockout (KO) screening upon introducing exogenous dsRNAs. Subsequent exploration of viral infection within the dsRNA interactome unveiled previously unrecognized dsRBPs that mitigate viral replication. Collectively, our methodology presents valuable resources in studying dsRNA regulation in physiological and pathological states.

Results

Identification of putative dsRBPs in human cells

Previous studies by our and other groups revealed that SINE-derived RNAs occupy the most abundant class of cellular dsRNAs[6,31]. Considering that these SINE RNAs are about 300 nucleotides long while a typical dsRBP recognizes RNAs with 10 ~ 20 bp in length[32], we hypothesized that some of the double-stranded regions must be exposed even after the RNA is bound to proteins. To capture these dsRBPs systematically, we utilized a K1 antibody that recognizes dsRNAs longer than 40 bp[33]. In particular, the K1 antibody recognizes dsRNAs without sequence specificity, which enables the unbiased identification of dsRBPs associated with various cellular dsRNA species[33]. Our proposed strategy is presented in Fig. 1a, where we performed IP using magnetic protein A bead coated with K1 antibody and analyzed the co-IPed proteins via quantitative mass spectrometry.

We began our investigation by testing the feasibility of our approach. First, we examined the species of cellular dsRNAs bound by the K1 antibody by analyzing the RNAs captured by the antibody using RT-qPCR. We found that ERV (*ERVL*), several SINEs (*AluSx1_2158*, *AluSx1_2166*, *AluSg_2231*, and *AluSg_2276*), and LINE (*L1PA2* and *L1PA3*) were significantly enriched compared to glyceraldehyde 3-phosphate dehydrogenase (*GAPDH*) mRNA in the K1 IP samples (Fig. 1b). Of note, other RNAs all showed enrichment in the K1 IP samples, but did not show statistical significance due to large variation. In addition, we used an abundant ribosomal protein L15 (*RPL15*) mRNA as another control. Although *RPL15* mRNA did show significant enrichment, the degree of enrichment was much weaker than transposable element-derived dsRNAs (Fig. 1b). Next, we analyzed the protein eluates upon K1 IP to examine whether the well-known dsRBPs could be captured by our approach. We found that ADAR1, PKR, and STAU1 were all strongly enriched in K1 co-IPed eluate, whereas two abundantly expressed non-RBP controls, β-tubulin (TUBB) and GAPDH, were undetected (Fig. 1c). Moreover, the enrichment of the three tested dsRBPs was specific to K1 co-IPed eluate as they were weakly detected in animal-matched control and no antibody control eluates (Fig. 1c).

Encouraged by these results, we performed a large-scale K1 co-IP experiment for liquid chromatography-tandem mass spectrometry (LC-MS/MS) analysis. We identified 1183 proteins, of which 1121 belonged to the K1 captured sample and 1092 to the control sample with animal-matched IgG, with 1030 (87%) overlapping proteins (Fig. 1d). Statistical analysis showed good correlations among biological replicates and distinct characteristics between K1 and control groups in the PCA plot, adding to the reliability of our experimental results (Supplementary Fig. 1a, b). When we computed the enrichment for individual proteins, a substantial number of proteins showed positive fold change, indicating that these proteins are likely to be specifically enriched in K1 co-IPed eluates (Fig. 1e).

Among the K1 co-IPed proteins detected in all four biological replicates, we selected 148 proteins (p-values of less than 0.05 and a fold change over two compared to control groups) for further analysis (Fig. 1e, marked in orange). Interestingly, the protein activator of interferon-induced protein kinase EIF2AK2 (PRKRA), which contains two canonical dsRNA binding domains (dsRBDs), and STAU2, a paralog of STAU1, are strongly enriched, further confirming the reliability of our results. Of note, most of these proteins were not identified by the previous oligo-dT pull-down method, even when formaldehyde was used as a crosslinking reagent[25,34]. In addition, many RNA-associated proteins were specifically pulled down with the K1 antibody. For example, up-frameshift suppressor 1 homolog (UPF1), La-related protein 1 (LARP1), and LARP4 that can bind to structured elements in the 3′ UTRs were found. An unexpected finding was 2, 4-dienoyl-CoA reductase 1 (DECR1), a mitochondrial metabolic enzyme involved in β-oxidation, as one of the most significantly enriched proteins.

As none of these proteins were previously associated with dsRNA-binding, we confirmed whether they are strongly and specifically pulled down by the K1 antibody via K1 IP followed by western blotting. Consistent with the LC-MS/MS results, our validation data clearly showed that the examined proteins are all enriched in the K1 co-IP eluate (Fig. 1f). In addition, we performed the same experiment in two additional cell lines (A549 lung adenocarcinoma cells and PC-3 prostatic adenocarcinoma cells), and found that all four examined putative dsRBPs were successfully captured by the K1 pull-down (Fig. 1f). Moreover, a similar enrichment pattern was observed when we used J2 antibody, another dsRNA binding antibody[33], to capture cellular dsRNAs (Fig. 1f). Alternatively, we performed a reciprocal experiment where we IPed the above four dsRBP candidates and examined the co-IPed dsRNAs using J2 dot blot assay. As a positive control, we used PKR, which showed strong J2 signals from the PKR co-IPed RNAs (Fig. 1g). Although the strength of the signal was quite different, all four dsRBP candidates showed J2 signal stronger than the negative control

(RNAs co-IPed with animal-matched IgG) (Fig. 1g). Of note, since the efficiency of each antibody in capturing their target protein is different as shown in Fig. 1h, we cannot conclude that the J2 signal reflects the dsRNA-binding affinities of these proteins.

Characterization of K1 captured proteins

To analyze the biological characteristics of the proteins captured by the K1 antibody, we first conducted a gene ontology (GO) analysis on molecular function. Consulting GO annotations of 148 proteins revealed that 14 proteins were annotated with 'dsRNA binding' (Fig. 2a). A significant portion of the remaining proteins (115 out of 134) was labeled with 'RNA binding', and 16 proteins were not previously associated with RNAs (Fig. 2a). Of note, many of these 148 proteins were ribosomal proteins, which likely reflects the fact that some ribosomal RNAs (rRNAs) were inevitably pulled down with dsRNAs due to their high abundance. Therefore, we removed small and large ribosomal subunit proteins as well as

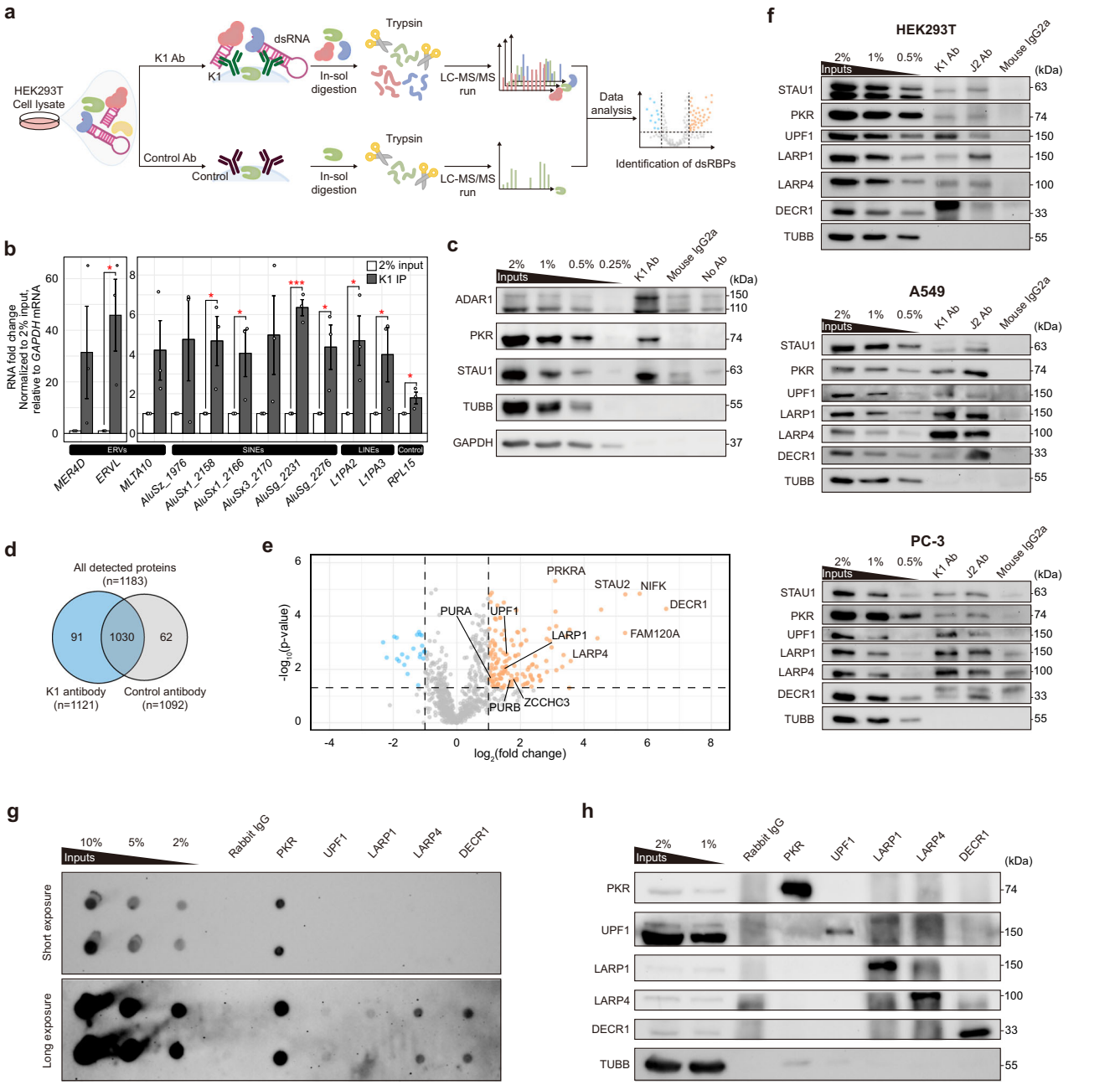

Fig. 1 | Capture of dsRNA interacting proteins with K1 antibody. a Schematics of the K1 IP followed by LC-MS/MS to identify proteins bound to cellular dsRNAs. **b** Enrichment levels of representative cellular dsRNA species in RNAs co-IPed with the K1 antibody. An average of three biological replicates is shown with error bars denoting s.e.m. Statistical significances were calculated using a one-sided Student's t-test; $^{*}p < 0.05$ and $^{***}p < 0.001$. **c** Western blotting analysis comparing K1 and control antibody captured protein samples. **d** Summary of the number of proteins identified in K1 or control antibody capture. **e** A volcano plot of proteins identified in all four K1 capture replicates. Significantly enriched proteins ($\log_2$(fold change) ≥ 1 and p-value < 0.05) are marked in orange while significantly depleted proteins are marked in blue. The $\log_2$(fold change) was calculated as the difference between the averaged $\log_2$(LFQ intensity) of four replicates in each experimental group. Statistical significances were calculated using two-sided Student's t-tests after false discovery rate (FDR) adjustments according to Benjamini-Hochberg at a 0.05 threshold. **f** Western blot validation for selected proteins identified through the K1 capture in three different cell lines. **g** J2 dot blot analysis of RNAs co-IPed with PKR and selected dsRBP candidates. **h** Western blotting analysis to check the IP efficiency of the antibodies used in **g**.

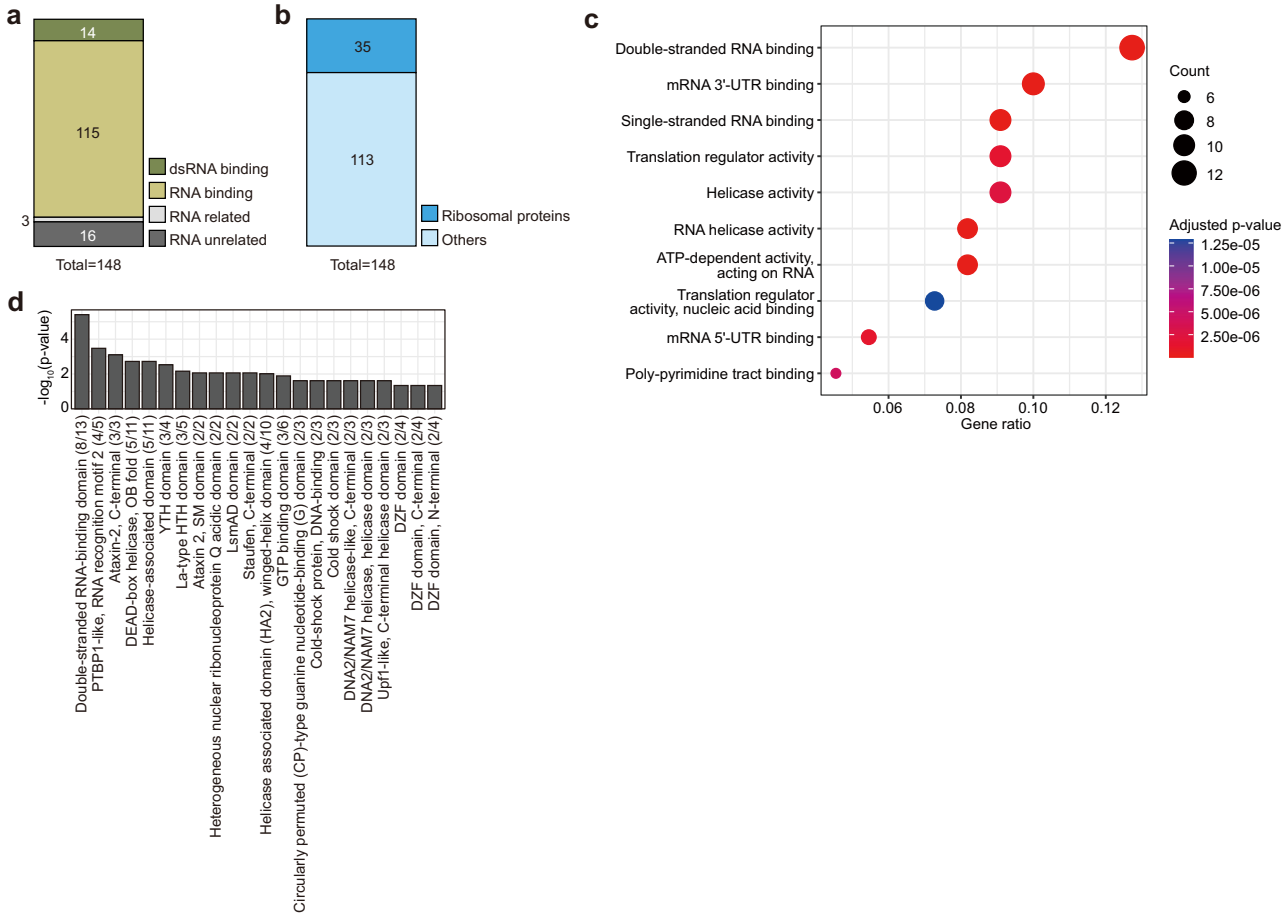

Fig. 2 | Characterization of K1 captured proteins. a Categorization of identified candidate dsRBPs based on GO terms in molecular function. **b** Number of ribosomal subunit proteins in the identified list. **c** A dot plot illustrating the enriched GO terms in molecular function among 113 candidate dsRBPs from the K1 interactome, excluding ribosomal subunits, analyzed using the clusterProfiler R package. **d** Significantly enriched protein domains and their respective p-values are shown. Numbers in the parentheses correspond to the number of proteins with the domain in the K1 interactome compared to all proteins detected in LC-MS/MS.

mitochondrial ribosomal proteins (35 proteins) from our list for further analysis (Fig. 2b). We denoted the remaining 113 proteins as the "K1 interactome" (Supplementary Data 1).

Enrichment analysis with GO on the molecular function of the identified K1 interactome also revealed various RNA-related terms as top hits, including 'mRNA 3′-UTR binding' and 'Single-stranded RNA binding'. Notably, 'Double-stranded RNA binding' was the most significantly enriched term (Fig. 2c). Domain enrichment analysis based on InterPro domain annotations revealed significant enrichment of RNA binding domains and helicase domains (Fig. 2d). In addition, proteins containing well-known RNA-interacting domains, such as 'PTBP1-like, RNA recognition motif 2', 'YTH domain', and 'La-type HTH domain', were detected as well. In particular, 'Double-stranded RNA-binding domain' was the most significant enriched term. These results collectively confirmed that our K1 interactome reflects the cellular dsRNA interactome, including previously unappreciated proteins.

Validation of dsRNA binding capability of the K1 interactome

Many of the cellular dsRNAs are transcribed as a part of host RNAs. For example, most SINE-derived dsRNAs captured by the J2 antibody are embedded in introns and UTRs of protein-coding genes and are transcribed as a part of the host mRNA[31]. Consequently, our K1 interactome may contain RBPs that were bound in the single-stranded region in the vicinity of the dsRNA structure that was recognized by the K1 antibody. To exclude such a possibility and improve the accuracy of our putative dsRNA interactome, we performed two additional LC-MS/MS analyses (Fig. 3a).

First, we treated cell lysates with RNase T1, an endonuclease that cleaves after guanine residue of ssRNAs, during the IP step with the K1 antibody. The addition of the RNase T1 enzyme would ensure that RNA captured by the K1 antibody is fully double-stranded and remove contaminating ssRNA interactors. Feasibility test with K1 IP followed by western blotting showed that canonical dsRBPs, such as ADAR1, STAU1, and PKR, showed enhanced enrichment in RNase T1-treated samples (Fig. 3b). LARP1, one of the putative dsRBPs identified by the K1 pull-down assay, also retained moderate enrichment in RNase T1-treated samples. Although the degree of enrichment decreased, it is clearly higher than that of the animal-matched IgG control (Fig. 3b). As a ssRNA-binding control, we used embryonic lethal, abnormal vision-like RNA binding protein 1 (ELAVL1) that recognizes AU-rich region in the 3′ UTR[35]. Consistent with our expectation, RNase T1 treatment significantly reduced the enrichment of K1 co-IPed ELAVL1 (Fig. 3b). As a negative control, we again used TUBB and GAPDH, which were undetected in any of the samples analyzed (Fig. 3b).

We then prepared a large-scale RNase T1-treated K1 co-IPed sample for LC-MS/MS analysis. We performed LC-MS/MS analysis on four biological replicates, and statistical analysis showed good correlations between the replicates (Supplementary Fig. 2a). Of note, the correlation values between different experimental groups were less than those between K1 experimental and control groups (Supplementary Fig. 2a). This trend was consistent with the PCA plot showing clear clustering (Supplementary Fig. 2b). A total of 1096 proteins were detected, and notably, RNase T1 treatment yielded a higher number of significantly enriched proteins captured by K1 antibody compared to the animal-matched control (Fig. 3c). We believe that this result reflects an improved degree of enrichment for

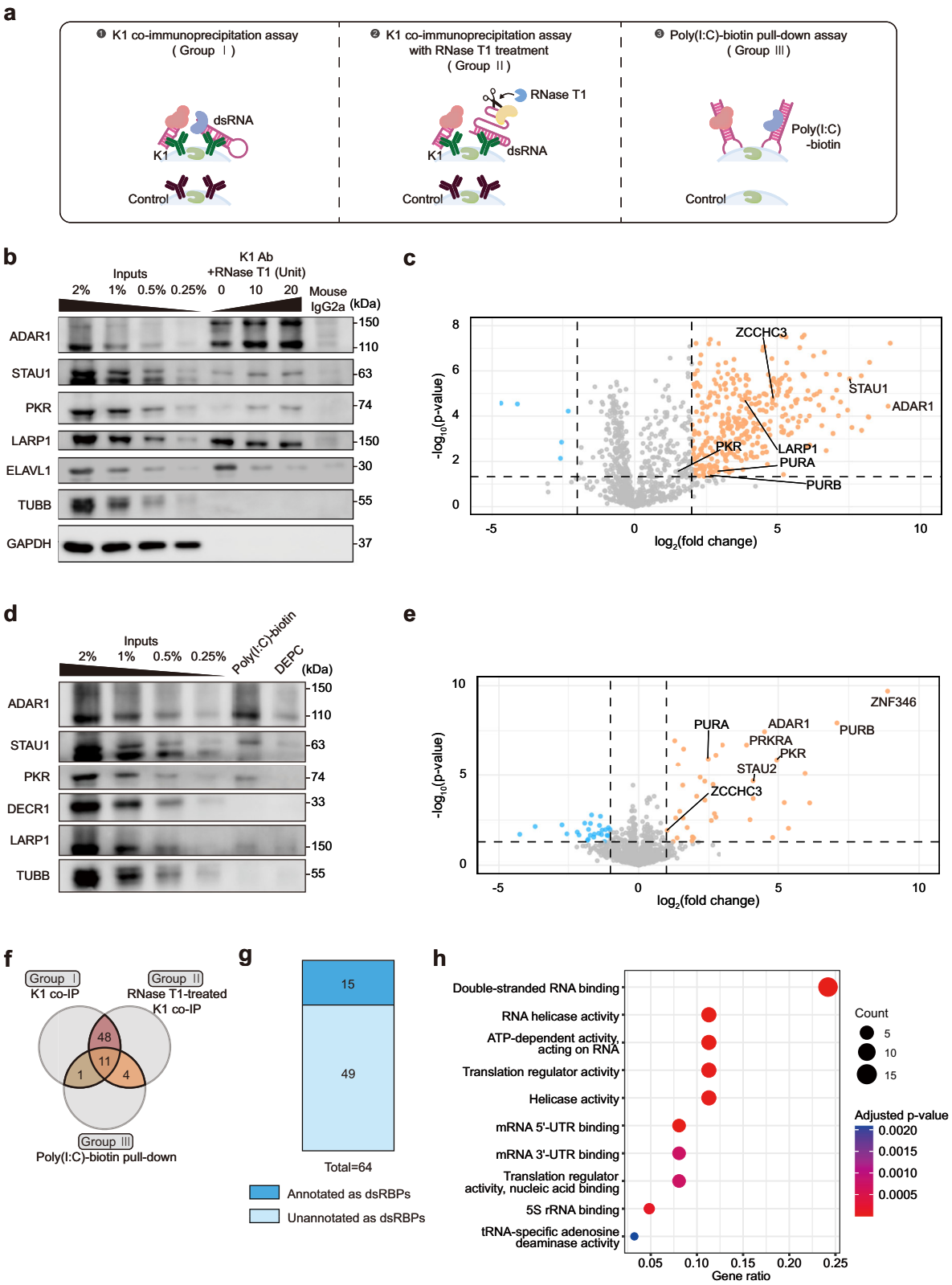

dsRBPs, as shown by the western blotting results of ADAR1, STAU1, and PKR when RNase T1 was treated (Fig. 3b). One possibility is that RNase T1 treatment reduced the ssRNA contaminants and short-structured RNAs that are recognized by the K1 antibody, hence resulting in improved signal-to-noise ratio for dsRBPs that interact with RNAs with extended stretch of double-stranded regions. As the RNase T1 treatment resulted in a large number of proteins that are significantly enriched in the K1 captured eluates, we used more stringent criteria (p-value less than 0.05 and a fold change of greater than four) to narrow down the list, which yielded 348 proteins. After excluding 76 ribosomal proteins, the GO analysis of the remaining 272 proteins annotated as RNase T1-treated K1 interactome revealed a significant enrichment of helicase-related GO terms, with the dsRNA binding GO term ranking fourth (Supplementary Fig. 2c, d; Supplementary Data 2).

Fig. 3 | K1 capture with RNase T1 treatment and poly(I:C) pull-down assay. **a** Schematics of two additional strategies in identifying potential dsRBPs using RNase T1 treatment in the K1 IP and poly(I:C) pull-down followed by LC-MS/MS. **b** Western blot showing selected K1 captured proteins after RNase T1 treatment during the IP step. **c** A volcano plot depicting the proteins captured by K1 with RNase T1 treatment, along with the mass spectrometry. Proteins that satisfy the filtering criteria with i) $\log_2$(fold change) ≥ 2 and ii) p-value < 0.05 are depicted in orange. Log_2(fold change) was calculated as the difference between the averaged $\log_2$(LFQ intensity) of four biological replicates in each experimental group. Statistical significances were calculated using two-sided Student's t-tests after false discovery rate (FDR) adjustments according to Benjamini-Hochberg at a 0.05 threshold. **d** Western blot of selected K1 captured proteins in poly(I:C) pull-down eluates. **e** A volcano plot showing poly(I:C) pull-down followed by LC-MS/MS results. Proteins that satisfy the filtering criteria with i) $\log_2$(fold change) ≥ 1 and ii) p-value < 0.05 are depicted in orange. Log_2(fold change) was calculated as the difference between the averaged $\log_2$(LFQ intensity) of four biological replicates in each experimental group. Statistical significances were calculated using two-sided Student's t-tests after FDR adjustments according to Benjamini-Hochberg at a 0.05 threshold. **f** Overlaps between the original K1 capture, RNase T1-treated K1 capture, and poly(I:C) pull-down proteins. **g** The number of previously annotated dsRBPs captured in our dsRNA interactome. **h** A dot plot illustrating the enriched GO terms in molecular function of the dsRNA interactome analyzed using the clusterProfiler R package.

Second, we utilized synthetic dsRNAs, poly(I:C), to compare the poly(I:C)-interacting proteins with the K1 interactome (Fig. 3a). Of note, for the poly(I:C) capture, we incubated biotinylated poly(I:C) with cell lysates in vitro instead of transfecting poly(I:C) into the cell to capture proteins with dsRNA-binding potential without any restriction in their subcellular localization. Prior to LC-MS/MS analysis, we performed a feasibility test by incubating cell lysate with magnetic beads coated with biotinylated poly(I:C) and analyzing proteins bound to poly(I:C) via western blotting. Well-known dsRBPs (ADAR1, STAU1, and PKR) again showed good enrichment compared to control without poly(I:C) while TUBB did not show any enrichment (Fig. 3d). Interestingly, proteins from the K1 interactome exhibited quite variable results. DECR1 was no longer detected in poly(I:C) pulled-down samples, while LARP1 showed a moderate affinity for poly(I:C) (Fig. 3d).

Mass spectrometry analysis of the poly(I:C) bound proteome revealed high enrichment of several dsRBPs, such as ADAR1, PKR, PRKRA, and STAU2, and showed a good correlation between biological replicates as well as distinguishable clusters in PCA analysis (Fig. 3e; Supplementary Fig. 3a, b). We identified 38 proteins meeting the criteria of p-value less than 0.05 and a fold change greater than two. Excluding one ribosomal protein, 37 proteins were designated as constituents of the poly(I:C) interactome, of which 12 were well-documented dsRBPs (Supplementary Fig. 3c; Supplementary Data 3). The GO analysis highlighted dsRNA binding as the most significantly enriched term within this poly(I:C) interactome (Supplementary Fig. 3d).

The interactomes obtained through the aforementioned three methods represent proteins capable of binding to different types of dsRNA ligands, albeit sharing a common potential for dsRNA binding. Proteins such as purine-rich element binding protein A (PURA), purine-rich element binding protein B (PURB), and zinc finger CCHC-type containing 3 (ZCCHC3) showed strong enrichment in all three types of LC-MS/MS analyses (Supplementary Fig. 4). In the process of discovering potential dsRNA interactomes without restricting the dsRNA ligand to poly(I:C), we selected proteins present in the interactomes in at least two of the three methods and denoted them as "dsRNA interactome" (Fig. 3f; Supplementary Fig. 4). A total of 64 proteins, including 15 previously annotated dsRBPs, were obtained (Fig. 3g). The GO analysis of these 64 proteins showed typical features of dsRBPs, such as 'Double-stranded RNA binding' (Fig. 3h). Therefore, we subjected these proteins to further analysis of their potential functional role, as shown below.

Putative dsRBPs can regulate IFN response to poly(I:C) stimulation and affect the replication of the HCoV-OC43 virus

Currently, the most well-characterized function of dsRNA interacting proteins is innate immunity, such as type I IFN response, to non-self RNAs. For instance, RIG-I and MDA5 serve as cytosolic viral dsRNA sensors that trigger RLR-mediated IFN response[16], while ADAR1 disrupts dsRNAs through A-to-I editing to suppress autoimmune response to self-RNAs[22]. Thus, we envisioned that many of the newly identified dsRBP candidates might also regulate the type I IFN response when exogenous RNAs were introduced. To test, we carried out a CRISPR-Cas9-based loss-of-function screening in response to poly(I:C) transfection using secreted IFN-β level and cell viability as readouts (Fig. 4a). Of note, we switched our experimental system to A549 cells because HEK293T cells showed too weak response to poly(I:C) transfection (Supplementary Fig. 5a, b).

Two sgRNAs were designed for each of the 32 genes curated from the dsRNA interactome to KO its expression. Of note, we selected 31 proteins out of 64 based on their reported molecular function and we used RIG-I as a positive control. We first validated the experimental robustness by employing the well-known cytosolic dsRNA sensor, RIG-I. A mixture of three non-target (NT) sgRNAs that have no matching sequence in the entire human genome was used as a negative control. The high indel frequency at the genome level and the reduction in protein expression at the protein level in each generated KO cell confirmed that employing two sgRNAs per gene is sufficient to draw near complete removal of the targets (Fig. 4b, c). Of note, we checked the protein expression of UPF1 as UPF1 showed one of the lowest indel frequencies of 49%, and our western results showed a near-complete reduction in the protein expression (Fig. 4c).

We then transfected 1 ng/ml of poly(I:C) and measured secreted IFN-β levels from individual KO cells via ELISA assay. Tolerance towards the cytotoxic effect of poly(I:C) was also assessed by measuring the remaining cell population with the cell counting kit-8 (CCK-8) assay (Fig. 4d, e). We found that KO of most genes resulted in significantly reduced levels of IFN-β compared to NT control (Fig. 4d). One notable gene was zinc finger CCCH-type antiviral 1 protein (ZC3HAV1), which has been shown to suppress translation and facilitate the degradation of viral mRNA[36]. Our screening result also showed decreased IFN-β secretion to poly(I:C) stimulation in ZC3HAV1 KO cells. On the contrary, in cells where YTH N^6-methyladenosine RNA binding protein C2 (YTHDC2), family with sequence similarity 120 member A (FAM120A), insulin-like growth factor 2 mRNA binding protein 3 (IGF2BP3), and Mov10 RNA helicase (MOV10) KO, the release of IFN-β in response to poly(I:C) was enhanced. In particular, YTHDC2 and IGF2BP3 are reader proteins that recognize N^6-methyladenosine (m^6A)-modified RNAs, influencing the fate of mRNA and RNA metabolism[37]. Furthermore, we observed that cells exhibiting hyper-activated IFN-β response were more susceptible to poly(I:C)-induced cell death, whereas cells with suppressed IFN-β response showed relatively less occurrence of cell death (Fig. 4e). In other words, the IFN-β concentration in response to poly(I:C) and the cell survival rate induced by poly(I:C) showed a negative correlation (Fig. 4f).

Considering that these putative dsRBPs can also bind and regulate cellular dsRNAs, we examined the effect of dsRBP KO on IFN-β secretion without poly(I:C) stimulation. We analyzed the changes in *IFNB1* and several ISG mRNA levels in cells seven days after sgRNA lentivirus transduction. Of note, the ISGs were chosen based on their high degree of induction in our previous studies, where we performed transcriptome-wide profiling upon poly(I:C) stimulation[13,38]. We found that *IFNB1* and many ISGs were upregulated in most KO cells, although the degree of induction was small (Supplementary Fig. 6a, b). We further examined phosphorylation of PKR and interferon regulatory factor 3 (IRF3), a key downstream factor of MDA5 and RIG-I, in YTHDC2, IGF2BP3, UPF1, and RIG-I KO cells as these cells showed the largest changes in ISG expression. Consistent with the increased levels of ISGs, we found PKR and IRF3 activation in YTHDC2 and IGF2BP3, but not in UPF1 KO

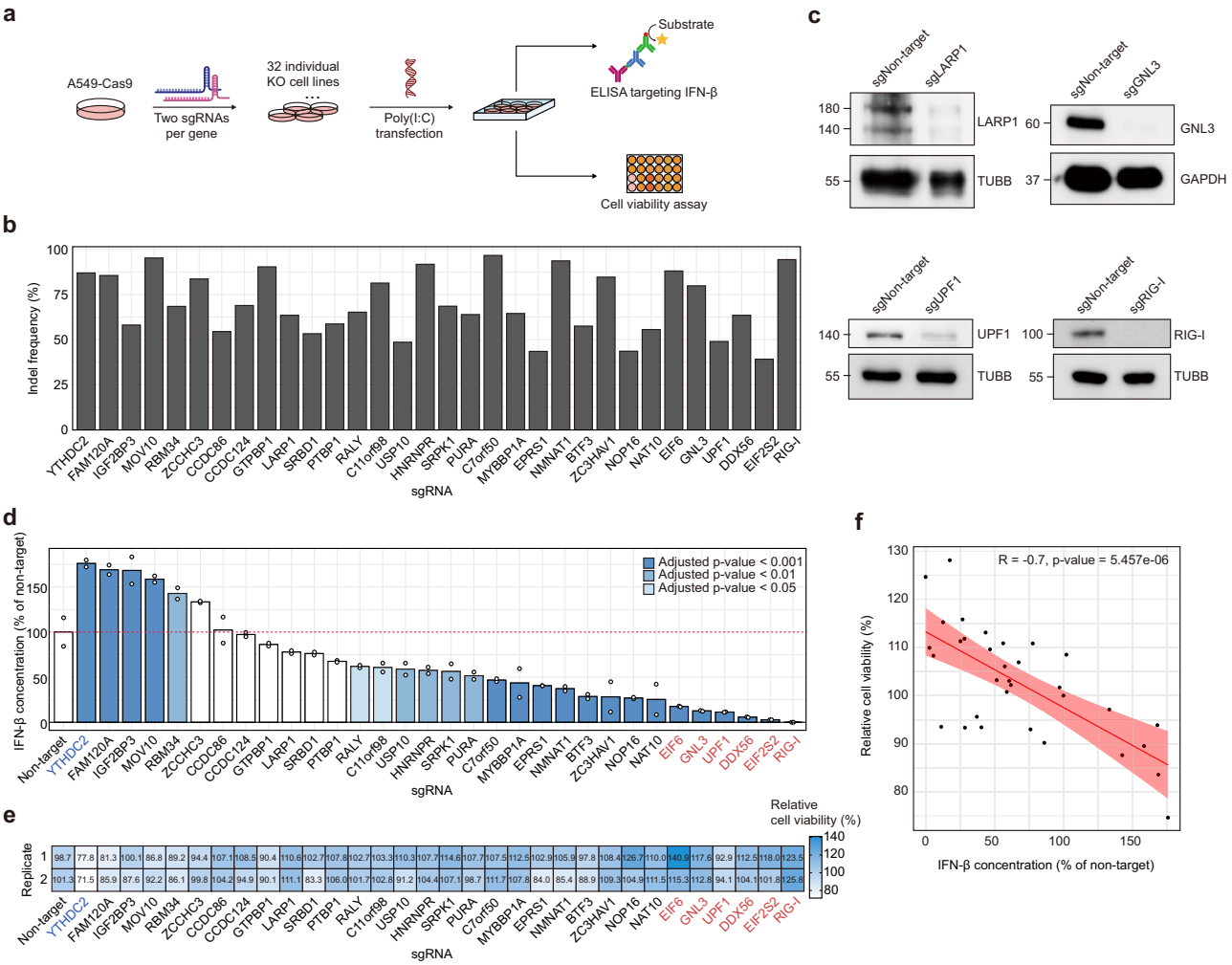

Fig. 4 | The immunoregulatory potential of the dsRNA interactome. a Schematics of the CRISPR screening procedures. Each gene in the dsRNA interactome was targeted with a mixture of two sgRNAs. The KO cells were treated with poly(I:C), and secreted IFN-β level and cell viability were analyzed as readouts. **b**, **c** Validation of the KO efficiency with high throughput target DNA sequencing (**b**) and western blotting of selected proteins (**c**). **d** Normalized secreted IFN-β levels in the dsRBP candidate KO cells compared to non-target (NT) control. Genes whose KO resulted in a significant change in IFN-β expression are shown as dark blue. An average of two biological replicates are shown with error bars denoting s.e.m. Statistical significances were calculated using a one-way ANOVA with Dunnett's post-hoc test, and the color of the bar indicates adjusted p-values. **e** The effect of poly(I:C) transfection in the indicated KO cells on cell viability, normalized against that of the NT cells. **f** Pearson correlation between IFN-β level and cell viability. Pearson's *r* was calculated using R version 4.2.1 (http://www.r-project.org).

cells, indicating that UPF1 may regulate ISG expression in a dsRNA-independent manner (Supplementary Fig. 6c). These findings suggest that the identified dsRBPs may modulate downstream signaling of endogenous dsRNA sensing.

Lastly, we investigated the potential anti- or proviral roles of the putative dsRBPs. We focused on the genes that showed the most significant changes in secreted IFN-β levels. Specifically, we selected one gene with the largest increase in IFN-β expression and five genes with the most significant decrease in IFN-β induction. We then examined the effect of knocking out these genes in the replication of HCoV-OC43, a positive-sense, single-stranded RNA virus that generates dsRNA intermediates during its replication and transcription processes[39] (Fig. 5a). Before analyzing the effect of dsRBP candidate KO on HCoV-OC43 replication, we tested whether HCoV-OC43 infection also induces IFN-β similar to that of poly(I:C) stimulation. Our data clearly showed that 1 ng/ml of poly(I:C) transfection results in a slightly higher degree of *IFNB1* mRNA induction and IFN-β secretion than those of 48 h after HCoV-OC43 infection with a multiplicity of infection (MOI) of one (Fig. 5b, c). The degree of selected ISG induction showed a similar pattern as *IFNB1* mRNA (Fig. 5d, e). Of note, *IFNB1*, ISGs, and IFN-β secretion did not show significant change 12 hours post infection (h.p.i) (Supplementary Fig. 7a-c).

With these data, we analyzed the effect of dsRBP KO on the replication of HCoV-OC43 48 h.p.i. As a positive control, we used RIG-I, whose KO resulted in enhanced viral replication. We found that eukaryotic translation initiation factor 6 (EIF6), G protein nucleolar 3 (GNL3), and DEAD-box helicase 56 (DDX56) KO cells exhibited an increase in viral replication over time, which is consistent with their effect of decreased IFN-β levels (Fig. 5f). On the other hand, KO of YTHDC2, which exhibited an enhanced IFN-β secretion to poly(I:C), slightly decreased the viral replication (Fig. 5f). Notably, the effect of HCoV-OC43 replication, for the most part, mirrored the effect of IFN-β secretion in response to poly(I:C) stimulation, suggesting that the dsRBP candidates may influence the cellular antiviral response by regulating dsRNA-mediated IFN response, thereby impacting the viral replication.

Discussion

In this study, we report a systematic and comprehensive effort to elucidate a repertoire of proteins that interact with cellular dsRNAs by directly capturing proteins bound to dsRNAs using K1 antibody. Such method was employed to overcome the limitations of low UV crosslinking efficiency between dsRNA and dsRBP and to characterize dsRBPs that can interact with diverse classes of cellular dsRNAs rather than a single specific RNA

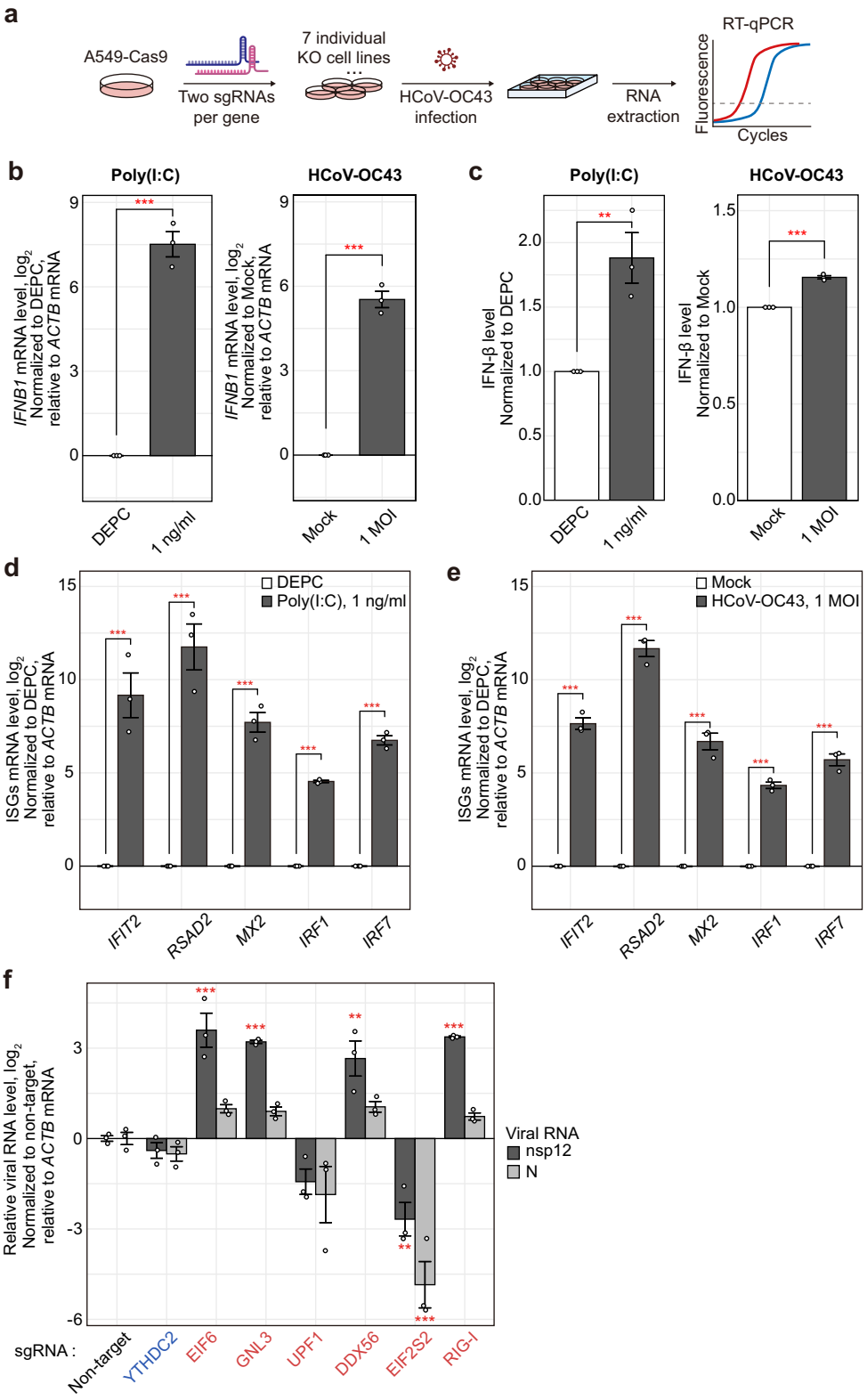

Fig. 5 | Regulation of viral replication by the dsRNA interactome. a Schematics HCoV-OC43 infection in A549-Cas9 cells with a specific dsRBP candidate expression depleted. **b**, **c** Comparison of *IFNB1* mRNA (**b**) and secreted IFN-β (**c**) levels between poly(I:C) stimulation and HCoV-OC43 infection 48 h.p.i. **d**, **e** Comparison of selected ISG mRNA induction between poly(I:C) stimulation (**d**) and HCoV-OC43 infection 48 h.p.i (**e**). For (**b**)–(**e**), statistical significances were calculated using one-sided Student's t-test; $^{**}p < 0.01$ and $^{***}p < 0.001$. **f** Change in nsp12 gRNA and N sgRNA levels measured by RT-qPCR in the indicated KO cells 48 h.p.i. In all bar graphs, an average of three biological replicates are shown with error bars denoting s.e.m. For (**f**), viral RNA levels from sgNT transduced cells served as the control. Statistical significances were calculated using a one-way ANOVA with Dunnett's post-hoc test; **adjusted $p < 0.01$ and ***adjusted $p < 0.001$.

bait. We further improved the reliability of our K1 interactome by utilizing RNase T1 to remove ssRNA-bound proteins and by employing in vitro binding to poly(I:C) as a canonical dsRNA to capture interacting proteins. In the end, we discovered 64 putative dsRBPs, denoted as dsRNA interactome. We further investigated the functional role of selected dsRBP candidates via CRISPR-Cas9 KO screening with IFN-β and cell viability as readouts. Interestingly, we found that the KO of most dsRBPs resulted in decreased sensitivity to a dsRNA stressor (e.g., poly(I:C)), indicating that these proteins might function as mediators of innate immunity during exogenous RNA sensing. Indeed, we showed that cells deficient in many of these proteins are more vulnerable to HCoV-OC43 virus infection, underscoring the significance of dsRBP-mediated immune regulation.

Our study provides valuable resources and insights into the cellular dsRNA interactome. For instance, two of the proteins whose KO enhanced IFN-β levels to poly(I:C) stimulation were m^{6}A readers, YTHDC2 and IGF2BP3. Previously, studies showed the potential role of m^{6}A modification on innate immunity where m^{6}A writer methyltransferase 3 (METTL3) induces RNA methylation to prevent dsRNA formation while m^{6}A reader YTH N^6-methyladenosine RNA binding protein F2 (YTHDF2) recognizes m^{6}A modified dsRNAs to facilitate their degradation[40]. Moreover, reports have indicated that disturbances in the m^{6}A machinery result in changes in the spread of various viruses due to irregular methylation of viral RNAs[41], and it is speculated that the m^{6}A readers, YTHDC2 and IGF2BP3, may be involved in this response. Our data support that m^{6}A modification may occur on cellular dsRNAs as m^{6}A readers are captured by the K1 antibody. In addition, the increased IFN-β levels to poly(I:C) stress in cells deficient in YTHDC2 and IGF2BP3 further suggest that the removal of m^{6}A-modified RNAs by these reader proteins can affect innate immunity during exogenous RNA sensing. Of note, since poly(I:C) cannot be methylated, our results indicate that basal dsRNA expression may affect the sensitivity of exogenous RNA sensing and that RNA modifications may regulate the basal dsRNA level and eventually affect cellular defense against viral infection. Indeed, we have shown that m^{5}C modification can mark dsRNAs for decay[42]. This effect of cellular dsRNA affecting viral response is further supported by a recent report where depletion of ELAVL1 and ELAVL2 decreased the level of endogenous dsRNAs via 3′ UTR shortening, which subsequently increased vulnerability to herpes simplex virus and zika virus infection in neurons[43]. In addition, considering that METTL3 can directly modify viral RNAs, the removal of m^{6}A-modified dsRNAs by the readers might be an evolved viral defense mechanism[44]. Interestingly, the KO of YTHDC2 resulted in the initial enhancement of HCoV-OC43 viral replication that is eventually suppressed over time. Further investigation is required to delineate the potential selectivity of m^{6}A modification on dsRNAs and its role in innate immunity to cellular dsRNAs.

Based on our CRISPR screening results, the depletion of EIF2S2 and UPF1 was expected to enhance virus replication. Instead, EIF2S2 and UPF1 KO cells showed decreased viral replication 48 h.p.i. Although the exact mechanism is unclear, we can speculate a few possibilities. For EIF2S2, we observed that its KO greatly reduced cell proliferation, which may be related to its function as a translation initiation factor. Consequently, the viral replication could be more strongly influenced by decreased cell proliferation rather than decreased IFN-β secretion in EIF2S2 KO cells. For UPF1, we cannot rule out the effect of the key function of UPF1 in RNA surveillance, in particular in mediating nonsense-mediated decay. For example, it is possible that UPF1 may directly regulate the expression of proviral genes, which may affect viral replication.

Our dsRNA interactome includes several proteins associated with stress granules, such as G3BP2 and LSM12[45–47]. Notably, our pull-down experiments were conducted in HEK293T cells without any stress granule-inducing stimuli. Yet, our data clearly suggest that stress granule components are bound to cellular dsRNAs and captured in K1 IP. This result is consistent with a recent study that showed aged mRNAs are bound by stress granule proteins even without granule formation[48]. In addition, our findings provide insights in understanding recently reported dsRNA-induced foci (dRIFs), which serve as an activation center for antiviral response to exogenous dsRNAs[49]. Indeed, nearly all of the reported components of dRIFs (PKR, ADAR1, PACT, STAU1, and DHX9) were detected in our K1 capture and exhibited strong binding to the poly(I:C) RNAs. Therefore, it is worthwhile to investigate whether other dsRBP candidates identified in our study are also associated with dRIFs and the possibility of regulating dRIF formation and maintenance. Collectively, our results provide valuable resources in investigating factors that may contribute to the liquid-liquid phase transition during stress conditions.

Lastly, we found many proteins that were previously shown to directly interact with viral RNAs and regulate their replication. A previous study showed that ZCCHC3 binds to viral RNAs and facilitates the recognition of these RNAs by RIG-I-like receptors[50]. Our finding suggests that ZCCHC3 may also bind to cellular dsRNAs and regulate their recognition by dsRNA sensors to regulate the downstream IFN response. In addition, we were surprised to see LARP1 on our list. Recent studies showed that LARP1 directly binds to SARS-CoV-2 RNA and regulates the downstream immune response[28,29]. Based on our results, it is possible that LARP1 recognizes dsRNAs or dsRNA-like structured RNAs and promotes their recognition by dsRNA sensors.

While this extensive dataset provides interesting insights into the dsRNA interactome, it is subject to several limitations that necessitate further investigation. Our study was mainly based on dsRNA capture using the K1 antibody and could not provide specific interacting dsRNA species for individual dsRBP candidates. Considering the biophysical nature of dsRNA-RBP interaction that RBPs recognize the structural features of the dsRNA due to the narrow major groove of the A-form helix of the dsRNA[16], it is likely that our putative dsRBPs will bind to SINE-derived dsRNAs. However, due to subcellular localization or liquid-liquid phase transition, certain dsRBPs will preferentially bind to a selective class of dsRNAs. The dsRNA substrates of the identified putative dsRBPs need to be discovered through methods such as formaldehyde crosslinking immunoprecipitation and sequencing. In addition, our results might contain pseudo-dsRBPs that were inadvertently co-eluted with protein complexes formed via protein-protein interactions. For example, our list contains many proteins involved in stress granule formation. Although many of these proteins are shown to have RNA-binding properties, their direct interaction with dsRNAs must be examined individually before concluding that these proteins are indeed dsRBPs. Moreover, the subcellular localization of dsRBP candidates, together with their interacting dsRNAs, needs to be examined as our method cannot exclude the possibility that certain proteins came into contact with dsRNAs during the IP step rather than inside the cell. Due to the sensitivity issue of LC-MS/MS, there will be numerous false negatives, especially for less abundant dsRBPs. Removing ribosome contamination either by treating cells with translation initiation inhibitors, such as homoharringtonine, or directly removing ribosomes using a sucrose cushion may result in the identification of additional dsRBPs. Lastly, the K1 antibody can detect proteins binding to dsRNA molecules with helices longer than 40 bp, making K1 insufficient to capture proteins binding to short dsRNAs. Particularly, these short dsRNAs can serve as agonists for RIG-I[16]. Moreover, for dsRNAs to be recognized by K1, proteins must not cover the entire dsRNA and exclude regions to allow the K1 antibody to bind on the same RNA molecule. Perhaps, these are the reasons why our list lacks RIG-I and MDA5, as the latter oligomerizes along the dsRNA and may occupy the entire dsRNA[51].

Despite these limitations, our study highlights previously unappreciated potential dsRBPs that play central roles in modulating the antiviral response during exogenous RNA sensing and viral infection. We provide valuable resources of putative dsRBPs for future investigation, and our approach can be further extended to various physiological and pathological contexts to broaden our understanding of dsRNA biology.

Methods

K1 IP for western blotting or LC-MS/MS analysis

Cells were cultured on a 150 mm plate per sample and harvested using a scraper. The collected cell pellet was washed twice with cold dulbecco's phosphate-buffered saline (DPBS). 50 µl of protein A magnetic beads (Bioneer) were washed once with 300 µl of the IP buffer (136 mM NaCl, 5 mM KCl, 0.7 mM Na_2HPO_4, and 25 mM Tris-Cl) supplemented with 1% NP40 and incubated with 10 µg of the K1 antibody (Cell Signaling Technology) or an animal-matched control antibody (Cell Signaling Technology) in the IP buffer for 3 h at 4 °C with rotation. On the ice, the cell pellet was resuspended in the IP buffer (136 mM NaCl, 5 mM KCl, 0.7 mM Na_2HPO_4, and 25 mM Tris-Cl) supplemented with 1% NP40, protease inhibitor cocktail (Thermo Fisher Scientific), and RNase inhibitor (Takara). After several pipetting, the mixture was passed through a syringe by repeatedly injecting and ejecting it 100 times through a 26 G needle. 50 µl of

antibody-coated magnetic protein A beads were washed twice with the IP buffer with 1% NP40 and incubated with 300 µl of the lysate with a concentration of 10 µg/µl for 3 h at 4 °C with rotation. The beads were washed three times with the IP buffer with 1% NP40 and then centrifuged to remove the supernatant. To analyze the sample for western blotting, 50 µl of 2X SDS-PAGE loading buffer was added to the bead, thoroughly vortexed, and incubated at 95 °C for 10 min. The samples were then loaded onto an SDS-PAGE gel for further analysis.

For the LC-MS/MS sample, beads were resuspended in the elution buffer (8 M urea in 50 mM ammonium bicarbonate (ABC)) and incubated at RT overnight with shaking in a thermomixer (Eppendorf) at 600 rpm. The sample was centrifuged, and the supernatant was analyzed for LC-MS/MS.

For the RNase T1-treated K1 co-IP experiment, samples were prepared using the same method as above, except for two modifications. First, cells were lysed with the IP buffer with 1% NP40 and protease inhibitor cocktail but without RNase inhibitor. Second, during the IP step, lysate was added to the bead together with 20 units of RNase T1 (Worthington) for 3 h at 4 °C with rotation.

In vitro capture of poly(I:C) binding proteins

For in vitro capture of poly(I:C)-binding proteins, cell lysates were collected and washed twice with ice-cold DPBS. Cells were lysed with ice-cold IP buffer containing 1% NP40 and protease inhibitor cocktail and incubated on ice for 10 min. Cells were then sonicated for complete lysis and to obtain cell lysates without any residual subcellular organelles and proteins in a bare state. The cell lysate was then centrifuged at 4 °C for 10 min, and the supernatant was collected. Streptavidin magnetic beads (Bioneer) were prepared by washing once with the IP buffer containing 1% NP40. Beads were then incubated with biotin-poly(I:C) conjugates (Thermo Fisher Scientific) for 3 h at 4 °C. After incubation, beads were washed three times with fresh IP buffer containing 1% NP40. Approximately 3 mg of prepared lysate was incubated with the beads at 4 °C for 3 h, and the beads were washed three times with the IP buffer containing 1% NP40, followed by two additional washes using the IP buffer without NP40. Samples were eluted with either 2X SDS-PAGE loading buffer (for western botting) or elution buffer (for LC-MS/MS). For western blotting, the sample was boiled at 95 °C for 10 min before loading onto an SDS-PAGE gel.

LC-MS/MS analysis

In-house packing of both analytical capillary columns (100 cm × 75 µm i.d.) and trap columns (2 cm × 150 µm i.d.) utilized 3 µm Jupiter C18 particles (Phenomenex). A consistent column temperature of 45 °C for the long analytical column was achieved through the use of a dedicated column heater (Analytical Sales and Services). Chromatographic elution was performed using a NanoAcquity UPLC system (Waters) at a flow rate of 300 nl/min over a total run time of 150 min, which included a linear gradient over 100 min, transitioning from 95% solvent A (0.1% formic acid in water) to 40% solvent B (0.1% formic acid in acetonitrile). Two mass spectrometers were employed for LC-MS/MS analysis, both equipped with a specialized nanoelectrospray ion source designed in-house: the Orbitrap Eclipse and the Orbitrap Fusion Lumos (Thermo Fisher Scientific). The setup for the Orbitrap Eclipse involved acquiring precursor ions within an m/z range of 300–1500 at a resolution of 120 K. Isolation of the precursor for MS/MS analysis was performed using a 1.4 Th. High-energy collisional dissociation (HCD) for peptide sequencing was applied at an energy setting of 30%. MS2 scans were performed at a resolution of 30 K, targeting an AGC of 1×10^5 with a maximum ion injection time (ITmax) of 54 ms. For the Orbitrap Fusion Lumos, the settings were an m/z range of 300–1800 at a resolution of 60 K, MS2 scans at a resolution of 7.5 K, an AGC target of 5×10^4, and an ITmax of 22 ms. The mass spectrometry proteomics data have been deposited to the ProteomeXchange Consortium via the PRIDE[52] partner repository with the dataset identifier PXD053100 and 10.6019/PXD053100 (Supplementary Data 4).

Protein identification of the dsRNA interactome

The MS/MS data were analyzed using MaxQuant software (version 2.0.3.0) with the Andromeda search engine against the SwissProt Homo sapiens proteome database (version 2023.01, with 20,404 entries; Uniprot (http://www.uniprot.org/)). Mass tolerances of 10 ppm for precursor ions and 20 ppm for fragmentation ions were applied. The label-free quantitation (LFQ) and matching between runs were executed with specified search criteria: trypsin digestion, allowing up to 2 missed cleavages, fixed modification of carbamidomethylation at cysteine sites, and variable modifications of acetylation at protein N-termini, oxidation at methionine. The PERSEUS software was utilized as the statistical tool for identifying proteins within the dsRNA interactome and for quantitative assessment. LFQ intensities were log-transformed following the exclusion of reverse sequences and contamination. Protein groups reporting a minimum of two LFQ intensities under at least a single experimental group were included in subsequent analyses. Missing LFQ values were substituted using imputation from a normal distribution.

Statistics and reproducibility

For the identification of dsRNA interactome, a Student's t-test with false discovery rate (FDR) adjustments according to Benjamini-Hochberg at a 0.05 threshold was employed for the statistical evaluation of protein groups. The same statistical methodology was used to investigate differentially captured protein groups within dsRNA interactomes. For cell studies, statistical analysis was performed with the Microsoft Excel 2016 software and GraphPad Prism10. Statistical significance was determined using one-sided tests and calculated using Student's t-tests, except for the screening data, which was processed by an ANOVA with Dunnett's post-hoc test. P value < 0.05 was considered as statistically significant ($^*p < 0.05$, $^{**}p < 0.01$, and $^{***}p < 0.001$). All data are presented as mean ± s.e.m. and sample size n is presented in the figure legends.

Generation of polyclonal dsRBP KO cells

Cas9-BLAST and lentiGuide-Puro inserted sgRNA plasmids were designed and packaged into lentiviral vectors (psPAX2 and pMD2.G) following protocols described in previous studies[53,54]. To delete the target gene expression, two sgRNAs were designed, and a mixture of two kinds of lentiviruses containing each sgRNA was transduced into Cas9-expressing A549 cells, supplemented with 5 µg/ml polybrene (Sigma-Aldrich) to enhance transduction. The sequences of sgRNAs are listed in Supplementary Data 5. 24 h post-transduction, cells were selected with puromycin at 5 µg/ml concentration, and the media was refreshed every other day. At seven days post-transduction, the KO efficiency was confirmed via high-throughput DNA sequencing and western blotting.

High-throughput DNA sequencing

The cell pellet was resuspended in 100 µl proteinase K extraction buffer (40 mM Tris-HCl (pH 8.0), 1% Tween-20, 0.2 mM EDTA, 2 mg proteinase K, 0.2% NP40 (VWR)). The resuspended pellet was incubated at 60 °C for 15 min, followed by 98 °C for 5 min. PCR amplification was then carried out with KOD-Multi & Epi- (TOYOBO) according to the manufacturer's protocol using 2 µl of genomic DNA as a template. The 1 µl of PCR product was subjected to next PCR amplification using primers containing next-generation sequencing adaptors. The primer sequences used for PCR are listed in Supplementary Data 6. The PCR products were purified using a PCR purification kit (GeneAll) and then analyzed using an Illumina MiniSeq instrument. The sequencing results were analyzed using Cas-Analyzer software (http://www.rgenome.net/cas-analyzer/)[55].

Virus propagation and infection

For HCoV-OC43 propagation, 5×10^6 HCT-8 cells were seeded into T-75 flasks and stabilized for 24 h. Cells were rinsed twice with warm DPBS and then exposed to 3 ml of virus-diluted media without FBS at a concentration of 0.05 MOI, as determined by plaque assay (see below), for 1 h at 35 °C.

Following infection, the media containing the virus was substituted with reduced-serum media with 5% FBS, and cells were incubated at 35 °C until harvesting. Five days post-virus infection, the media were collected and centrifuged at 1000 g for 15 min at 4 °C.

The titer of propagated HCoV-OC43 was measured by plaque assay using a 12-well plate with 5×10^5 RD cells seeded. 300 µl of virus solution, diluted by a factor of 10, was used to infect the cells for 1 h without FBS, followed by overlaying with 0.75% agarose with high strength and low melting point containing reduced-serum media with 5% FBS. After five days, the number of plaques was visualized by staining with 2% crystal violet (Sigma-Aldrich), counted, and the titer was calculated.

For HCoV-OC43 infection, 4×10^5 cells were seeded in a 6-well plate and incubated with 5% CO_2 at 37 °C for one day. Cells were washed twice with warm DPBS, and the culture media was replaced with 500 µl of virus-diluted media without FBS at 1 MOI and incubated at 35 °C for 1 h. The plate was shaken every 10 min to prevent the cells from drying. Infected cells were washed one more time and replaced with reduced-serum media containing 5% FBS and incubated at 35 °C for 12 h or 48 h before harvesting.

Reporting summary

Further information on research design is available in the Nature Portfolio Reporting Summary linked to this article.

Data availability

Original western blot images are available at Mendeley (DOI: 10.17632/jdkgjszfc5.1). The mass spectrometry proteomics data have been deposited to the ProteomeXchange Consortium via the PRIDE partner repository with the dataset identifier PXD053100. Metadata associated with individual raw files can be found in PRIDE or Supplementary Data 4. The source data of all cell line experiments in the paper can be found in Supplementary Data 7. All relevant data are available from the authors upon reasonable request.

Code availability

We did not generate any new code.

Received: 25 July 2024; Accepted: 25 February 2025;
Published online: 07 March 2025

References

1. Pettersson, U. & Philipson, L. Synthesis of complementary RNA sequences during productive adenovirus infection. *P Natl. Acad. Sci. USA* **71**, 4887–4891 (1974).
2. Schlee, M. & Hartmann, G. Discriminating self from non-self in nucleic acid sensing. *Nat. Rev. Immunol.* **16**, 566–580 (2016).
3. Athanasiadis, A., Rich, A. & Maas, S. Widespread A-to-I RNA editing of alu-containing mRNAs in the human transcriptome. *Plos Biol.* **2**, 2144–2158 (2004).
4. Yoon, J., Kim, S., Lee, M. H. Y. & Kim, Y. Mitochondrial nucleic acids in innate immunity and beyond. *Exp. Mol. Med.* **55**, 2553–2563 (2023).
5. Lee, K., Ku, J., Ku, D. & Kim, Y. Inverted *Alu* repeats: friends or foes in the human transcriptome. *Exp. Mol. Med.* **56**, 1250–1262 (2024).
6. Lander, E. S. et al. Initial sequencing and analysis of the human genome. *Nature* **409**, 860–921 (2001).
7. Kim, S., Ku, Y., Ku, J. & Kim, Y. Evidence of aberrant immune response by endogenous double-stranded RNAs: attack from within. *Bioessays* **41**, e1900023 (2019).
8. Young, P. G. & Attardi, G. Characterization of double-stranded-RNA from hela-cell mitochondria. *Biochem Bioph Res Co.* **65**, 1201–1207 (1975).
9. Kang, M. et al. Double-stranded RNA induction as a potential dynamic biomarker for DNA-demethylating agents. *Mol. Ther. Nucl. Acids* **29**, 370–383 (2022).
10. Kim, Y. et al. PKR is activated by cellular dsRNAs during mitosis and acts as a mitotic regulator. *Gene Dev.* **28**, 1310–1322 (2014).
11. Kim, S. et al. Mitochondrial double-stranded RNAs govern the stress response in chondrocytes to promote osteoarthritis development. *Cell Rep.* **40**, 111178 (2022).
12. Lee, H. et al. Cell type-specific transcriptomics reveals that mutant huntingtin leads to mitochondrial RNA release and neuronal innate immune activation. *Neuron* **107**, 891–908.e8 (2020).
13. Yoon, J. et al. Mitochondrial double-stranded RNAs as a pivotal mediator in the pathogenesis of Sjögren's syndrome. *Mol. Ther.-Nucl. Acids* **30**, 257–269 (2022).
14. Chung, H. C. et al. Human ADAR1 prevents endogenous RNA from triggering translational shutdown. *Cell* **172**, 811–824.e14 (2018).
15. Kaneko, H. et al. DICER1 deficit induces *Alu* RNA toxicity in age-related macular degeneration. *Nature* **471**, 325–330 (2011).
16. Hur, S. Double-stranded RNA sensors and modulators in innate immunity. *Annu Rev. Immunol.* **37**, 349–375 (2019).
17. Hornung, V. et al. 5′-triphosphate RNA is the ligand for RIG-I. *Science* **314**, 994–997 (2006).
18. Peisley, A. & Hur, S. Multi-level regulation of cellular recognition of viral dsRNA. *Cell Mol. Life Sci.* **70**, 1949–1963 (2013).
19. Aktas, T. et al. DHX9 suppresses RNA processing defects originating from the *Alu* invasion of the human genome. *Nature* **544**, 115–119 (2017).
20. Kim, Y. et al. PKR senses nuclear and mitochondrial signals by interacting with endogenous double-stranded RNAs. *Mol. Cell* **71**, 1051–1063.e6 (2018).
21. Ku, Y. et al. Noncanonical immune response to the inhibition of DNA methylation by Staufen1 via stabilization of endogenous retrovirus RNAs. *P Natl. Acad. Sci. USA* **118**, e2016289118 (2021).
22. Cottrell, K. A., Andrews, R. J. & Bass, B. L. The competitive landscape of the dsRNA world. *Mol. Cell* **84**, 107–119 (2024).
23. Cottrell, K. A. et al. Induction of viral mimicry upon loss of DHX9 and ADAR1 in breast cancer cells. *Cancer Res Commun.* **4**, 986–1003 (2024).
24. Castello, A. et al. Insights into RNA biology from an atlas of mammalian mRNA-binding proteins. *Cell* **149**, 1393–1406 (2012).
25. Kwon, S. C. et al. The RNA-binding protein repertoire of embryonic stem cells. *Nat. Struct. Mol. Biol.* **20**, 1122–1130 (2013).
26. Kim, B., Jeong, K. & Kim, V. N. Genome-wide mapping of DROSHA cleavage sites on primary microRNAs and noncanonical substrates. *Mol. Cell* **66**, 258–269.e5 (2017).
27. Girardi, E. et al. Proteomics-based determination of double-stranded RNA interactome reveals known and new factors involved in Sindbis virus infection. *Rna* **29**, 361–375 (2023).
28. Lee, S. et al. The SARS-CoV-2 RNA interactome. *Mol. Cell* **81**, 2838–2850.e6 (2021).
29. Schmidt, N. et al. The SARS-CoV-2 RNA-protein interactome in infected human cells. *Nat. Microbiol* **6**, 339–353 (2021).
30. Uchida, L. et al. The dengue virus conceals double-stranded RNA in the intracellular membrane to escape from an interferon response. *Sci. Rep.-Uk* **4**, 7395 (2014).
31. Ku, J. et al. Alternative polyadenylation determines the functional landscape of inverted Alu repeats. *Mol. Cell* **84**, 1062–1077.e1069 (2024).
32. Tian, B., Bevilacqua, P. C., Diegelman-Parente, A. & Mathews, M. B. The double-stranded-RNA-binding motif: Interference and much more. *Nat. Rev. Mol. Cell Bio* **5**, 1013–1023 (2004).
33. Schonborn, J. et al. Monoclonal-antibodies to double-stranded-RNA as probes of RNA structure in crude nucleic-acid extracts. *Nucleic Acids Res* **19**, 2993–3000 (1991).
34. Na, Y. et al. FAX-RIC enables robust profiling of dynamic RNP complex formation in multicellular organisms. *Nucleic Acids Res.* **49**, e28 (2021).
35. Rothamel, K. et al. ELAVL1 primarily couples mRNA stability with the 3′ UTRs of interferon-stimulated genes. *Cell Rep.* **35**, 109178 (2021).

36. Zhu, Y. P. et al. Zinc-finger antiviral protein inhibits HIV-1 infection by selectively targeting multiply spliced viral mRNAs for degradation. *P Natl. Acad. Sci. USA* **108**, 15834–15839 (2011).
37. Jung, I. H. & Kim, Y. K. Exon junction complex is a molecular compass of N^6-methyladenosine modification. *Mol. Cells* **46**, 589–591 (2023).
38. Ku, D. et al. SLIRP mediates nuclear-mitochondrial communication during antiviral signaling to promote robust interferon response. *bioRxiv*, 2024.03.28.587146 (2024).
39. Xu, G. et al. Evidence for cross-species transmission of human coronavirus OC43 through bioinformatics and modeling infections in porcine intestinal organoids. *Vet. Microbiol* **293**, 110101 (2024).
40. Lee, Y., Choe, J., Park, O. H. & Kim, Y. K. Molecular mechanisms driving mRNA degradation by m6A modification. *Trends Genet* **36**, 177–188 (2020).
41. Zhang X. Y., Peng Q. & Wang L. J. N^6-methyladenosine modification-a key player in viral infection. *Cell Mol. Biol. Lett.* **28**, 78 (2023).
42. Kim, S. et al. RNA 5-methylcytosine marks mitochondrial double-stranded RNAs for degradation and cytosolic release. *Mol. Cell* **84**, 2935–2948.e7 (2024).
43. Dorrity, T. J. et al. Long 3′UTRs predispose neurons to inflammation by promoting immunostimulatory double-stranded RNA formation. *Sci. Immunol.* **8**, eadg2979 (2023).
44. Li, N. et al. METTL3 regulates viral m6A RNA modification and host cell innate immune responses during SARS-CoV-2 infection. *Cell Rep.* **35**, 109091 (2021).
45. Fischer, J. W., Busa, V. F., Shao, Y. & Leung, A. K. L. Structure-mediated RNA Decay by UPF1 and G3BP1. *Mol. Cell* **78**, 70–84.e76 (2020).
46. Matsuki, H. et al. Both G3BP1 and G3BP2 contribute to stress granule formation. *Genes Cells* **18**, 135–146 (2013).
47. Lee, J. et al. *LSM12-EPAC1* defines a neuroprotective pathway that sustains the nucleocytoplasmic RAN gradient. *Plos Biol.* **18**, e3001002 (2020).
48. Choi, Y. et al. Time-resolved profiling of RNA binding proteins throughout the mRNA life cycle. *Mol. Cell* **84**, 1764–1782 (2024).
49. Corbet, G. A., Burke, J. M., Bublitz, G. R., Tay, J. W. & Parker, R. dsRNA-induced condensation of antiviral proteins modulates PKR activity. *P Natl. Acad. Sci. USA* **119**, e2204235119 (2022).
50. Lian, H. et al. The Zinc-Finger Protein ZCCHC3 binds RNA and facilitates viral RNA sensing and activation of the RIG-I-like receptors. *Immunity* **49**, 438–448.e5 (2018).
51. Ahmad, S. et al. Breaching self-tolerance to alu duplex RNA underlies MDA5-mediated inflammation. *Cell* **172**, 797–810.e13 (2018).
52. Perez-Riverol, Y. et al. The PRIDE database resources in 2022: a hub for mass spectrometry-based proteomics evidences. *Nucleic Acids Res* **50**, D543–D552 (2022).
53. Hong, T., Bae, S. M., Song, G. & Lim, W. Guide for generating single-cell-derived knockout clones in mammalian cell lines using the CRISPR/Cas9 system. *Mol. Cells* **47**, 100087 (2024).
54. Shalem, O. et al. Genome-scale CRISPR-Cas9 knockout screening in human cells. *Science* **343**, 84–87 (2014).
55. Park, J., Lim, K., Kim, J. S. & Bae, S. Cas-analyzer: an online tool for assessing genome editing results using NGS data. *Bioinformatics* **33**, 286–288 (2017).

Acknowledgements

We thank all members of the Jong-Seo Kim, Sangsu Bae, and Yoosik Kim laboratory for helpful discussion and comments on the paper. We acknowledge the KAIST Analysis Center for Research Advancement for experimental equipment. This research was supported a grant of the Korea Dementia Research Project through the Korea Dementia Research Center (KDRC), funded by the Ministry of Health & Welfare and Ministry of Science and ICT (RS-2024-00346881) and the Bio & Medical Technology Development Program of the National Research Foundation (NRF) funded by the Korean government (MSIT) (RS-2024-00509338). J.-S.K. was supported by the Institute for Basic Science of the Ministry of Science and ICT of Korea (IBS-R008-D1).

Author contributions

J.L., N.L., S.J., and Y.K. designed the study and analysis. J.L., N.L., S.J., J.Kim., S.M., M.J., and S.-H.L. performed experiments. Y.-k.L. set up the virus experiment while J.Ku. assisted in establishing the K1 co-IP experiment. S.K. assisted in establishing the CRISPR screening. S. B. analyzed the high-throughput DNA sequencing results. J.-S.K. and Y.K. supervised the study. J.L., N.L., and Y.K. wrote the manuscript with contributions from S.J. and S.-H.L. All of the authors subsequently reviewed and edited the manuscript.

Competing interests

The authors declare no competing interests.

Additional information

Supplementary information The online version contains supplementary material available at https://doi.org/10.1038/s42003-025-07807-4.

Correspondence and requests for materials should be addressed to Jong-Seo Kim or Yoosik Kim.

Peer review information *Communications Biology* thanks Len Maggi, Shinichi Nakagawa and the other, anonymous, reviewer(s) for their contribution to the peer review of this work. Primary Handling Editors: Tuan Anh Nguyen and Mengtan Xing.